



# Evaluation of thermokinetics methodology, parameters, and coke characterization of co-pyrolysis of bituminous coal with herbaceous and agricultural biomass

Lin Mu<sup>1,2</sup> · Ranyu Wang<sup>1,2</sup> · Zhende Zhai<sup>1,2</sup> · Bin Zhang<sup>1,2</sup> · Yan Shang<sup>1,2</sup> · Hongchao Yin<sup>1,2</sup>

Received: 23 February 2021 / Revised: 29 March 2021 / Accepted: 6 April 2021 / Published online: 12 April 2021  
© The Author(s), under exclusive licence to Springer-Verlag GmbH Germany, part of Springer Nature 2021

## Abstract

In this paper, conventional thermogravimetric analysis and a new congruent–mass thermogravimetric analysis were used to study the reaction mechanism of the co-pyrolysis process of coal and biomass in the thermogravimetric analyzer, the effects of heating rate and carrier gas flow rate on co-pyrolysis were investigated, and kinetic analysis was conducted for the major pyrolysis stages to explore whether there was a synergistic effect in the co-pyrolysis process. The surface morphology of pyrolytic coke was evaluated by the fractal dimension method. The results show that congruent–mass thermogravimetric analysis can compare the interactions in the co-pyrolysis process more intuitively and reduce the influence of initial mass on the determination of interaction relationship. Synergistic effect appears in co-pyrolysis of coal and biomass. With the increase of heating rate, the thermogravimetric hysteresis appeared and the thermogravimetric curve gradually moved to the high temperature region. With the increase of carrier gas flow rate, the synergistic effect weakens. The kinetics of different reaction stages was analyzed by Coats–Redfern method; the results show that the activation energy required in the main co-pyrolysis stage of the mixture is lower than that in the pyrolysis stage alone. The micromorphology shows that biomass coke has a more developed pore structure than coal, and the box dimension indicates that co-pyrolysis increases the surface irregularity of coke. It is of great significance to judge the interaction mechanism of two or even multiple mixed samples in the process of co-pyrolysis.

**Keywords** Congruent–mass thermogravimetric analysis · Co-pyrolysis · Synergistic effect · Kinetic analysis · Fractal dimension

## 1 Introduction

The direct use of coal produces a large number of harmful substances, such as nitrogen oxides and sulfur dioxide, which are not only inefficient, but also cause irreversible damage to the environment [1]. Under the severe energy situation and pollutant emission situation, all countries in the world are vigorously developing clean coal technology and researching new renewable energy to reduce environmental pollution [2]. Biomass is abundant in sources and has the advantage of regeneration, and crop straw is rich in many kinds of elements,

high content of cellulose, hemicellulose, and lignin [3], and it is a kind of multi–purpose and renewable biological resource [4]. In China, about 900 million tons of crop stalks are produced every year, most of which are directly burned without efficient treatment and application, and the utilizable potential is huge. Crop production is derived from China Rural Statistical Yearbook (2020). Bamboo is a herbaceous plant and is the fastest growing plant in the world. It has great research and development value [5]. China ranks first in bamboo resources, area, and stock in the world. The annual output of bamboo exceeds 3 billion in China. Bamboo production is derived from China Forestry and Grassland Statistical Yearbook (2018).

Pyrolysis refers to the process in which solid material is heated to a certain temperature in an inert gas atmosphere, volatiles and tar are separated out, and coke or semi-coke is formed [6]. The ash content and fixed carbon content of coal are high, while biomass has a higher H/C ratio and ash contains more alkali metals. The co-reaction of coal and biomass can make full use of their advantages and improve the use

✉ Lin Mu  
l.mu@dlut.edu.cn

<sup>1</sup> School of Energy and Power Engineering, Dalian University of Technology, Dalian 116024, China

<sup>2</sup> Key Laboratory of Complex Energy Conversion and Utilization, Dalian 116024, Liaoning Province, China

efficiency [7–10]. The co-pyrolysis of coal and biomass is more complex than the single pyrolysis. Many scholars [11–18] have studied the interaction between the co-pyrolysis of coal and biomass. Park et al. [19] conducted co-pyrolysis experiments on wood chips and coal in thermogravimetric analyzer (TGA) and fixed-bed reactors; they found that above 400 °C, the weight loss rate of the wood chips and coal mixture increased, while more volatiles were released. Aboyade et al. [20] also obtained higher than expected volatile yield when studying the co-pyrolysis characteristics of bagasse and corn residue with coal. These studies show that there is synergy in the co-pyrolysis process. Wen et al. [21] also found in their co-combustion study of textile dyeing sludge (TDS) and incense sticks (IS) that the blend ratio of 25TDS/75IS exerted the most synergistic interaction effect that accelerated the reaction process. However, Idris et al. [22] found that the pyrolysis of the mixture of coal and oil palm biomass was independent from each other in the pyrolysis study of Malaysian sub-bituminous coal and three types of oil palm biomass in a thermogravimetric analyzer. Vhathvarothai et al. [23] also did not find obvious synergistic effect when studying the co-pyrolysis characteristics of nut shell and pine sawdust with bituminous coal. Zhang et al. [24] conducted co-gasification experiments on a variety of coal and biomass using a new congruent–mass thermogravimetric analysis method on TGA; no synergies were found in the early pyrolysis stage. It is worth noting that the high carrier gas flow rate may bring the volatile matter out directly. Therefore, it is effective to eliminate secondary gas–fuels reactions. Table 1 summarizes the experimental conditions and results of different scholars. By summarizing the experimental conditions of many scholars [25–27], it is found that the synergistic effect of co-pyrolysis process mainly occurs under the experimental conditions of appropriate or small carrier gas flow rate; the difference of carrier gas flow rate will affect the experimental results. The potential secondary gas–fuels reactions should be considered, especially in the application of large-scale pyrolysis processes.

In this study, pyrolysis of individual coal (Datong bituminous coal) or biomass (wheat straw and bamboo) sample, and co-pyrolysis experiments of coal and biomass were carried out in a thermogravimetric analyzer. Both conventional thermogravimetric analysis and congruent–mass thermogravimetric analysis methods were applied to comparative studies of the differential effects of these two methods on evaluation of potential interaction between the coal and biomass. In addition, the influence of heating rate and carrier gas flow rate on co-pyrolysis was investigated, the kinetics of the main pyrolysis stage were analyzed, and the surface morphologies of pyrolytic coke were evaluated by scanning electron microscope (SEM) and fractal dimension. The paper includes a new congruent–mass thermogravimetric analysis method that was applied in a TGA; comparative studies of the differential effects of two methods on

judging the interaction and surface morphologies of pyrolytic coke were evaluated by fractal dimension theory. It is of great significance to the determination of the interaction mechanism of two or more mixed samples in the co-pyrolysis process.

## 2 Experiment

### 2.1 Materials

One typical high volatile coal for gasification, Datong bituminous coal produced in Shanxi Province, China, was selected as the coal sample. The biomass samples were wheat straw from Shandong Province and bamboo from Sichuan Province. Wheat straw has a huge seasonal production in China, and bamboo is a potentially available biomass in the thermochemical conversion application [28, 29]. All the coal and biomass samples were crushed and dried, and the powders with particle size less than 0.2 mm were sieved as the experimental samples. Industrial analysis of coal and biomass was carried out in an AAF12/18 Muffle furnace produced by Carbolite Gero according to GB/T 212–2008 and GB/T 28731–2012. The elemental analysis of the samples was performed on the Vario Macro Cube elemental analyzer produced by Elementar. The calorific value of the samples was tested in the C2000 calorimeter produced by IKA. Table 2 shows the fuel properties of bituminous coal and biomass samples.

### 2.2 Experimental apparatus

The pyrolysis and co-pyrolysis thermogravimetric experiments were conducted in a TGA/DSC3+ synchronous thermal analyzer produced by Switzerland METTLER TOLEDO. The measurement range of temperature is from room temperature to 1600 °C. The balance has the high accuracy with the sensitivity of 0.01 µg. Figure 1 illustrates the schematic diagram of the balance in TGA/DSC3+. The balance holds two crucibles at the same time, which meets the requirement of two crucible simultaneously in congruent–mass thermogravimetric analysis. The morphology characteristics of pyrolyzed coke were analyzed by Sigma300 field emission scanning electron microscopy (SEM) produced by Zeiss.

### 2.3 Experimental methods and conditions

#### 2.3.1 Conventional thermogravimetric analysis

Firstly, a set of empty crucible experiments were conducted as the references to counteract the influence of physicochemical properties and buoyancy of crucible on the reaction during the heating processes. And then, 10 mg bituminous coal, 10 mg wheat straw, and 10 mg and 20 mg mixture of bituminous coal and wheat straw were pyrolyzed in the same crucible,

**Table 1** The experimental conditions and results of different scholars

| Scholars              | Materials                                                  | Experimental system          | Heating rate $\beta$ and atmosphere                                                                                                                                                       | Whether there is synergy |
|-----------------------|------------------------------------------------------------|------------------------------|-------------------------------------------------------------------------------------------------------------------------------------------------------------------------------------------|--------------------------|
| Du et al. [26]        | Bio-ferment residual, coal                                 | TG–FTIR                      | $\beta = 10, 30, 50 \text{ }^\circ\text{C}\cdot\text{min}^{-1}$ ;<br>1000 $^\circ\text{C}$ for 20 min;<br>$\text{N}_2, 50 \text{ ml}\cdot\text{min}^{-1}$ .                               | Yes                      |
| Wu et al. [27]        | Cellulose, carboxymethylcellulose sodium                   | TGA                          | $\beta = 10, 20, 40 \text{ }^\circ\text{C}\cdot\text{min}^{-1}$ ;<br>950 $^\circ\text{C}$ ;<br>$\text{N}_2, 60 \text{ ml}\cdot\text{min}^{-1}$ .                                          | Yes                      |
| Zhang et al. [24]     | Walnut shell, bituminous coal                              | TGA                          | $\beta = 10, 20, 40 \text{ }^\circ\text{C}\cdot\text{min}^{-1}$ ;<br>900 $^\circ\text{C}$ ;                                                                                               | No                       |
| Sadhukhan et al. [13] | Lignite coal, waste–wood fines                             | TG/DTA                       | $\text{N}_2, 200 \text{ ml}\cdot\text{min}^{-1}, \text{CO}_2, 200 \text{ ml}\cdot\text{min}^{-1}$<br>$\beta = 40 \text{ }^\circ\text{C}\cdot\text{min}^{-1}$ ;<br>1000 $^\circ\text{C}$ ; | No                       |
| Sonobe et al. [25]    | Thai lignite, corncob                                      | TGA, and a fixed-bed reactor | $\beta = 10 \text{ }^\circ\text{C}\cdot\text{min}^{-1}$ ;<br>300, 350, 400, 500, 600 $^\circ\text{C}$ for 30 min;<br>$\text{N}_2, 50 \text{ ml}\cdot\text{min}^{-1}$ .                    | Yes                      |
| Park et al. [19]      | Sawdust of larix leptolepis, sub-bituminous coal           | A fixed-bed reactor and TGA  | $\beta = 15, 30 \text{ }^\circ\text{C}\cdot\text{min}^{-1}$ ;<br>700, 900 $^\circ\text{C}$ ;<br>$\text{N}_2, 200 \text{ ml}\cdot\text{min}^{-1}$ .                                        | Yes                      |
| Masnadi et al. [15]   | Manitoba switchgrass, pine sawdust, Alberta Genesee coal   | High-pressure TGA            | $\beta = 25 \text{ }^\circ\text{C}\cdot\text{min}^{-1}$ ;<br>750, 800, 900 $^\circ\text{C}$ ;                                                                                             | No                       |
| Chen et al. [11]      | Microalgae chlorella vulgaris, coal                        | TGA                          | $\text{N}_2, 500 \text{ ml}\cdot\text{min}^{-1}; 100 \text{ bar}$ .<br>$\beta = 10, 20, 40 \text{ }^\circ\text{C}\cdot\text{min}^{-1}$ ;<br>1000 $^\circ\text{C}$ ;                       | Yes                      |
| Idris et al. [22]     | Low-rank Malaysian coal, oil palm biomass and their blends | TGA                          | $\text{N}_2, 100 \text{ ml}\cdot\text{min}^{-1}$ .<br>$\beta = 10, 20, 40, 60 \text{ }^\circ\text{C}\cdot\text{min}^{-1}$ ;<br>900 $^\circ\text{C}$ ; $\text{N}_2$ .                      | No                       |

respectively, and denoted as coal, wheat, CW10, and CW20 in sequence. The above experiments were repeated by replacing the biomass sample with bamboo, and the experiments were named as Bamboo, CB10, and CB20, respectively. In these experiment runs, the mixture rate of coal and biomass (wheat straw and bamboo) was 1:1 by weight. The pyrolysis processes were carried out under  $\text{N}_2$  atmosphere of  $q = 60 \text{ ml}\cdot\text{min}^{-1}$ . The experimental powders were heated up from room temperature to 900  $^\circ\text{C}$  at a heating rate of  $\beta = 50 \text{ }^\circ\text{C}\cdot\text{min}^{-1}$ , then kept for 10 min at 900  $^\circ\text{C}$ .

**2.3.2 Congruent–mass thermogravimetric analysis**

During the thermogravimetric experiment by the congruent–mass analysis method, pyrolysis of two empty crucibles under

the same condition was conducted as the reference in the thermogravimetric analyzer with the same purpose. And then these two crucibles were used throughout the following experimental procedures. The pyrolysis of samples included three experimental runs. In the first run, 10 mg coal and 10 mg wheat straw (QCW10+10) were put into the two crucibles, respectively, and pyrolyzed at the same time. For the second run, 20 mg mixture of coal and wheat straw (QCW20) was put into the two crucibles, and each crucible contained 10 mg of mixture. Furthermore, 40 mg (QCW40) mixture was used, and each crucible contained 20 mg. The same experiments were repeated by applying the experimental samples of coal and bamboo, and the runs were named as QCB10+10, QCB20, and QCB40. The temperature-controlled program and flow rate of the carrier gas were the same to those during

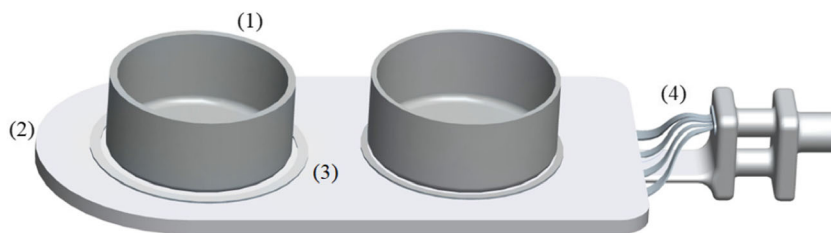
**Table 2** Proximate analysis, elemental analysis, and calorific value of coal and biomass

| Materials   | Proximate analysis/wt% |                 |                 |                         | Elemental analysis/wt% |                 |                 |                 |                 | Calorific value/ $\text{kJ}\cdot\text{kg}^{-1}$ |
|-------------|------------------------|-----------------|-----------------|-------------------------|------------------------|-----------------|-----------------|-----------------|-----------------|-------------------------------------------------|
|             | $M_{\text{ad}}$        | $A_{\text{ad}}$ | $V_{\text{ad}}$ | $\text{FC}_{\text{ad}}$ | $C_{\text{ad}}$        | $H_{\text{ad}}$ | $N_{\text{ad}}$ | $S_{\text{ad}}$ | $O_{\text{ad}}$ |                                                 |
| Coal        | 3.15                   | 6.71            | 35.84           | 54.30                   | 71.79                  | 2.79            | 0.97            | 0.26            | 24.19           | 27,694                                          |
| Wheat straw | 8.33                   | 11.53           | 66.89           | 13.25                   | 40.40                  | 3.51            | 0.65            | 0.48            | 54.96           | 16,209                                          |
| Bamboo      | 3.60                   | 0.65            | 81.96           | 13.79                   | 48.44                  | 3.97            | 0.24            | 0.23            | 47.12           | 18,872                                          |

The subscript ad stands for air dried basis:  $M_{\text{ad}} + A_{\text{ad}} + V_{\text{ad}} + \text{FC}_{\text{ad}} = 100$

The oxygen content was calculated by the difference method:  $O_{\text{ad}} = 100 - N_{\text{ad}} - C_{\text{ad}} - H_{\text{ad}} - S_{\text{ad}}$

**Fig. 1** TGA/DSC3+ type synchronous thermal analyzer balance sensor: (1) crucible, (2) balance cantilever, (3) thermocouples, and (4) sensors



the conventional analysis method. All the thermogravimetric experiments were carried out at least three times to guarantee the acceptable errors and reproducibility for each experiment run. Table 3 shows the experimental conditions and parameters.

### 2.3.3 Experimental conditions

For the integrated experimental scheme for the congruent-mass analysis method, the effects of heating rate and flow rate were considered. The mixture powders were heated at three different heating rates 10, 30, and 50 °C·min<sup>-1</sup>, and each crucible contained 10 mg mixture with N<sub>2</sub> atmosphere of 60 ml·min<sup>-1</sup>. And then, three different flow rates of N<sub>2</sub> (60, 100, and 200 ml·min<sup>-1</sup>) were set with the constant heating rate of 50 °C·min<sup>-1</sup> and final temperature of 900 °C. The initial sample weight of mixture was 20 mg as introduced in Section 2.3.2.

## 2.4 Data evaluation and analysis

### 2.4.1 Data evaluation

During the pyrolysis processes, it is assumed that there is no interaction between coal and biomass; therefore, the thermal weight loss of mixture samples is calculated by means of arithmetical average value, and the calculation formula is as follows:

$$M_{\text{calculated}} = M_{\text{Coal}} \times X_{\text{Coal}} + M_{\text{Biomass}} \times (1 - X_{\text{Coal}}) \quad (1)$$

where  $M_{\text{calculated}}$  is the arithmetical average results of separate pyrolysis of coal and biomass,  $M_{\text{Coal}}$  represents the real-time weight of coal in a single reaction process,  $M_{\text{Biomass}}$  represents the real-time weight of biomass in a single reaction process, and  $X_{\text{Coal}}$  represents the percentage of coal in the mixture.

For the conventional thermogravimetric method, relative weight difference  $\Delta M$  was used to describe the difference between the experimental and theoretical results of pyrolysis quantitatively. The calculation formula is as follows:

$$\Delta M = M_{\text{calculated}} - M_{\text{experimental}} \quad (2)$$

where  $M_{\text{experimental}}$  is the thermal weight loss obtained by the experiment run. If  $\Delta M$  is greater than zero, the co-pyrolysis process of coal and biomass shows the synergistic effect, while if  $\Delta M$  is less than zero, the inhibition effect occurs

during the co-pyrolysis process.  $\Delta M = 0$  means there is no synergy or inhibition effect.

For the congruent-mass thermogravimetric method,  $\Delta M$  is the mass-difference between individual pyrolysis and co-pyrolysis process.

The relative mass difference is quantified by root mean square (RMS), and obtained as follows:

$$RMS = \sqrt{\frac{\sum_{i=1}^n \Delta M_i^2}{n}} \quad (3)$$

Furthermore, the volatilization performance of the experimental powders during pyrolysis processes is evaluated by the transfer coefficient  $D_i$  [30], and obtained as:

$$D_i = \frac{R_{\text{max}}}{T_b \cdot T_{\text{max}} \cdot \Delta T_{1/2}} \quad (4)$$

where  $R_{\text{max}}$  is the maximum weight loss rate of the samples,  $T_b$  is the initial pyrolysis temperature; it is considered that the pyrolysis begins when the DTG curve is greater than 0.01%/s after the water volatilization process.  $T_{\text{max}}$  is the pyrolysis temperature corresponding to the maximum weight loss rate, and  $\Delta T_{1/2}$  represents the temperature range when the weight loss rate is half of the maximum weight loss rate.

### 2.4.2 Kinetic analysis

Thermal kinetics refers to the study of the physical properties, chemical reaction rate, and reaction mechanism of the substance under the isothermal or non-isothermal conditions by obtaining the reaction activation energy ( $E$ ) [31]. Kinetic analysis of pyrolysis reaction of coal and biomass is evaluated by the Coats–Redfern integral method and the activation energy calculated is the average value of the change of activation energy in each stage of pyrolysis.

According to the basic principles of thermokinetics, the relationship between reaction rate and time is expressed as:

$$\frac{d\alpha}{dt} = k(T) \cdot f(\alpha) \quad (5)$$

where  $t$  is the reaction time,  $f(\alpha)$  is the reaction mechanism function, and  $G(\alpha)$  is the integral form of  $f(\alpha)$ ; the calculation formula is as follows:

**Table 3** Experimental conditions and parameters

| Abbreviations | Materials          | Mass/<br>mg | Instructions                                                                                |
|---------------|--------------------|-------------|---------------------------------------------------------------------------------------------|
| Coal          | Coal               | 10          | One crucible contained 10 mg coal, and the other one was empty.                             |
| Wheat         | Wheat straw        | 10          | One crucible contained 10 mg wheat straw, and the other one was empty.                      |
| Bamboo        | Bamboo             | 10          | One crucible contained 10 mg bamboo, and the other one was empty.                           |
| CW10          | Coal + wheat straw | 5 + 5       | One crucible contained 10 mg mixture of coal and wheat straw, and the other cone was empty. |
| CW20          | Coal + wheat straw | 10 + 10     | One crucible contained 20 mg mixture of coal and wheat straw, and the other cone was empty. |
| CB10          | Coal+ bamboo       | 5 + 5       | One crucible contained 10 mg mixture of coal and bamboo, and the other cone was empty.      |
| CB20          | Coal+ bamboo       | 10 + 10     | One crucible contained 20 mg mixture of coal and bamboo, and the other cone was empty.      |
| QCW10+10      | Coal/wheat straw   | 10/10       | 10 mg coal and 10 mg wheat straw were put into the two crucibles respectively.              |
| QCW20         | Coal + wheat straw | 10 + 10     | 20 mg mixture was used, and each crucible contained 10 mg.                                  |
| QCW40         | Coal + wheat straw | 20 + 20     | 40 mg mixture was used, and each crucible contained 10 mg.                                  |
| QCB10+10      | Coal/bamboo        | 10/10       | 10 mg coal and 10 mg bamboo were put into the two crucibles respectively.                   |
| QCB20         | Coal + bamboo      | 10 + 10     | 20 mg mixture was used, and each crucible contained 10 mg.                                  |
| QCB40         | Coal + bamboo      | 20 + 20     | 40 mg mixture was used, and each crucible contained 10 mg.                                  |

$$G(\alpha) = \int \frac{1}{f(\alpha)} \cdot d\alpha \tag{6}$$

where  $\alpha$  is the sample conversion rate, which can be calculated by the following formula:

$$\alpha = \frac{m_0 - m_t}{m_0 - m_1} \tag{7}$$

where  $m_0$ ,  $m_t$ , and  $m_1$  are the initial sample mass, the sample mass at time  $t$ , and the residual mass after the heating procedure, respectively.  $k(T)$  is the reaction rate constant and obtained according to the Arrhenius formula:

$$k(T) = A \cdot \exp\left(-\frac{E}{RT}\right) \tag{8}$$

where  $E$  stands for the reaction activation energy,  $A$  is the pre-finger factor, and  $R = 8.314 \text{ J}\cdot\text{mol}^{-1}\cdot\text{K}^{-1}$  is the gas constant.

The heating rate  $\beta$  is a constant value for non-isothermal pyrolysis experiment, and the formula is as follows:

$$\beta = \frac{dT}{dt} \tag{9}$$

The kinetic analysis model is obtained by combining Eqs. (5)–(9):

$$\frac{d\alpha}{dT} = \frac{1}{\beta} A \cdot \exp\left(-\frac{E}{RT}\right) \cdot f(\alpha) \tag{10}$$

The most commonly used  $f(\alpha)$  formula at present is  $f(\alpha) = (1-\alpha)^n$ , in which  $n$  is the reaction series. Take the logarithm of both sides of Eqs. (10):

When  $n = 1$ ,

$$\ln \left[ \frac{-\ln(1-\alpha)}{T^2} \right] = \ln \left[ \frac{AR}{\beta E} \left( 1 - \frac{2RT}{E} \right) \right] - \frac{E}{RT} \tag{11}$$

When  $n \neq 1$ ,

$$\ln \left[ \frac{1-(1-\alpha)^{1-n}}{T^2(1-n)} \right] = \ln \left[ \frac{AR}{\beta E} \left( 1 - \frac{2RT}{E} \right) \right] - \frac{E}{RT} \tag{12}$$

The calculation of Eqs. (11) and (12) can be found in Refs. [32, 33]. The conversion rate  $\alpha_c$  is calculated by the fitting curve, and the  $\alpha_c$  obtained was compared with the sample conversion rate obtained from Eq. (7) to verify the fitting of kinetic parameters.

### 2.4.3 Coke morphology and fractal dimension

Fractal theory was an effective method to study the geometric and structural characteristics of surfaces. Fractal dimension can describe the complexity and irregular properties of surfaces [34]. The surface morphology of coal, wheat straw, and bamboo were evaluated by scanning electron microscope (SEM) and fractal dimension according to the fractal geometry. MATLAB was used to conduct in-depth analysis of the SEM images of pyrolysis products. Firstly, SEM image is converted into gray image in MATLAB and gray histogram is generated. In addition, the gray histogram is applied to evaluate an appropriate threshold to binarize the gray image. The generated logical data is imported into the Fraclab in order to obtain the double precision numeric

data. The appropriate scale is selected to calculate the box dimension  $D_s$  of the image [35]:

$$D_s = \frac{\ln(N_r)}{\ln(1/r)} \quad (15)$$

where  $D_s$  is the box dimension,  $r$  is the ruler selected during calculation, and  $N_r$  is the result under the determined criterion.

## 3 Results and discussion

### 3.1 Separate pyrolysis process of coal and biomass

Figure 2 illustrates the thermogravimetry (TG) and derivative thermogravimetry (DTG) curves of separate pyrolysis processes of coal and biomass. The DTG curve of coal has three obvious weight loss peaks, and the weight loss is relatively slow at 200–350 °C. The pyrolytic weight losses of bituminous coal consist of four stages. The weight loss process from room temperature to 200 °C is the first stage, and the main decomposition process is coal drying, dehydration, and removal of gases such as CO<sub>2</sub> and N<sub>2</sub> adsorbed on the surface; the weight loss peak appears at about 100 °C. The second stage is 200–350 °C corresponding to slow pyrolysis of coal. The relatively weak chemical bonds are broken, and functional groups such as carboxyl group and amide group are decomposed to releases small molecular gases such as CO and H<sub>2</sub>. The third stage is from 350 to 680 °C, which is the main coal degradation process; therefore, the TG curve drops sharply, and the DTG curve shows a significant weight loss peak around 500 °C. The large molecule side chain with stronger chemical bonds in coal is broken and removed. A large amount of volatiles are formed during this process. Meanwhile, the tar and gas species (CO, H<sub>2</sub>, CH<sub>4</sub>, and unsaturated gaseous hydrocarbon) are produced, accompanied by forming semi-coke. The fourth stage is 680–900 °C, and a third weight loss peak appears on the DTG curve around 860 °C. In this stage, secondary cracking and polycondensation occur on the surface of semi-coke or in the semi-coke, leading to the conversion of semi-coke to coke.

As illustrated in Fig. 2, the DTG curves of wheat and bamboo pyrolysis show three obvious weight loss peaks, which corresponds to the degradation processes of hemicellulose, cellulose, and lignin [36]. At the first stage between 120 and 200 °C, the main weight loss process is the evaporation of water inside the biomass. In addition, a small amount of CO, CO<sub>2</sub>, N<sub>2</sub>, and other small molecular substances is volatilized by the depolymerization and recombination reaction, and vitrification transformation process [37]. The second stage (190–400 °C) is the main process of the wheat straw and bamboo pyrolysis reaction. The TG curves of wheat straw and bamboo

decrease rapidly in a short time, and the pyrolysis reactions are violent and accompanied by the significant weight loss. At this stage, two obvious weight loss peaks appear in Fig. 2b. The temperature range between 200 and 240 °C is mainly the pyrolysis of hemicellulose, and the temperature range between 350 and 380 °C corresponds to intense decomposition of cellulose and lignin, producing a large amount of CO, H<sub>2</sub>, and other gases and volatiles. Most of hemicellulose and cellulose are basically converted into volatile components, and the main reaction process is carbonization caused by the degradation of lignin and unreacted solid residues when the reaction temperature above 400 °C. Compared with the main pyrolysis process, the TG curves moderate at this stage.

### 3.2 Comparative analysis between conventional analysis and congruent–mass analysis

Figure 3 illustrates the TG and DTG curves of mixture powders by the conventional thermogravimetric method. The calculated TG and DTG curves of mixture pyrolysis processes according to Fig. 2 are also presented in Fig. 3. As illustrated in Fig. 3a, under the same pyrolysis condition, the  $M_{\text{experimental}}$  curve of CW10 after 200 °C is lower than the weighted  $M_{\text{calculated}}$  curve. It means that the weight loss of the mixture during the pyrolysis is strengthened, and the final coke yield (40.36%) is lower than the theoretical value (43.14%). In addition, the weight loss rate of CW10 at the main pyrolysis stage is higher than that calculated by the weighting, and the pyrolysis process of CW10 shows a certain synergistic effect. However, the overall pyrolysis curve of CW20 is close to the theoretical calculation curve, the final coke yield (44.09%) is slightly higher than the theoretical coke yield, and the pyrolysis process is likely to be no interaction. As to the co-pyrolysis of coal and bamboo, similar results are obtained. By comparison, the calculated curves with experimental curves, the synergistic effect is found during the pyrolysis process of CB10, but not for the CB20 run.

For the conventional thermogravimetric analysis method, it is obvious that at the experimental runs CW10 and CB10, the total mass of the mixture is equal to the mass of each sample during the separate pyrolysis process, and the mass of each sample in the mixture is half of the total mass. While at the experimental runs CW20 and CB20, the weight of the individual sample is guaranteed to be equal, and the total mixture weight is twice that of the individual reactants. Due to the difference in the initial sample mass, the potential interaction between the mixed samples during the co-pyrolysis process results in differentiated results; it is difficult to discern a synergistic or inhibiting effect between the mixed samples. By using the congruent–mass thermogravimetric analysis method, only two groups of experiments, QCB10+10 and QCB20, can be used to directly compare whether the synergistic effect exists, which avoids the calculation of multiple groups of

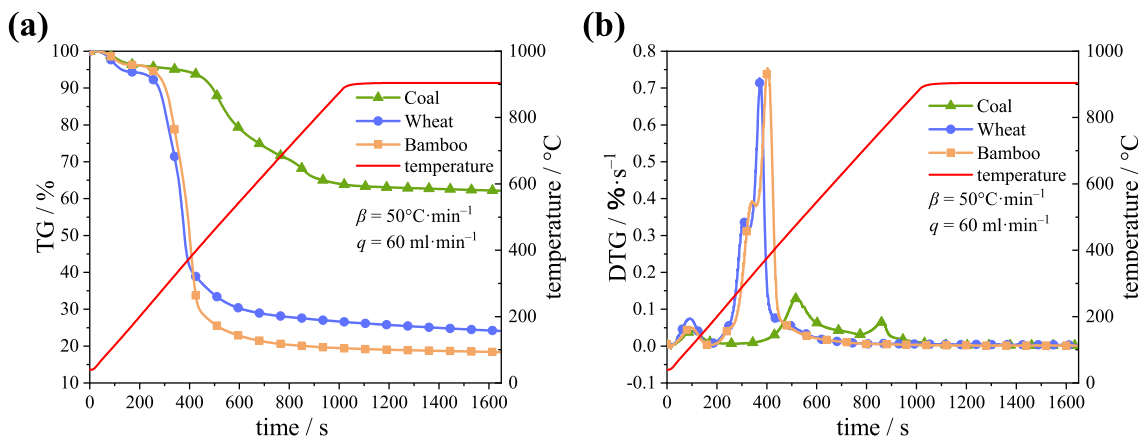


**Fig. 2** TG and DTG curves of coal and biomass separate pyrolysis based on the conventional thermogravimetric analysis method

experiments in the conventional thermogravimetric analysis method and the influence of initial mass selection on the determination. The method is deemed to compare the interactions during the co-pyrolysis process conveniently. And QCB20 and QCB40 were compared to verify the influence of initial quality on the pyrolysis reaction.

The pyrolysis TG and DTG curves of coal and biomass, and their mixture based on the congruent-mass thermogravimetric analysis method, are shown in Fig. 4. For the

experimental runs QCW10+10 and QCW20, it is guaranteed that the total mass of coal and biomass is equal in each group, and the mass of a single substance is also equal, as listed in Table 3. During the co-pyrolysis of coal and wheat straw (QCW20), as shown in Fig. 4a, when the heating temperature reaches the main pyrolysis temperature range of coal, the pyrolysis TG curve of QCW20 is significantly lower than that of QCW10+10. The relative quality difference  $\Delta M$  is greater than 0, and the *RMS* of relative mass difference is 2.64. The

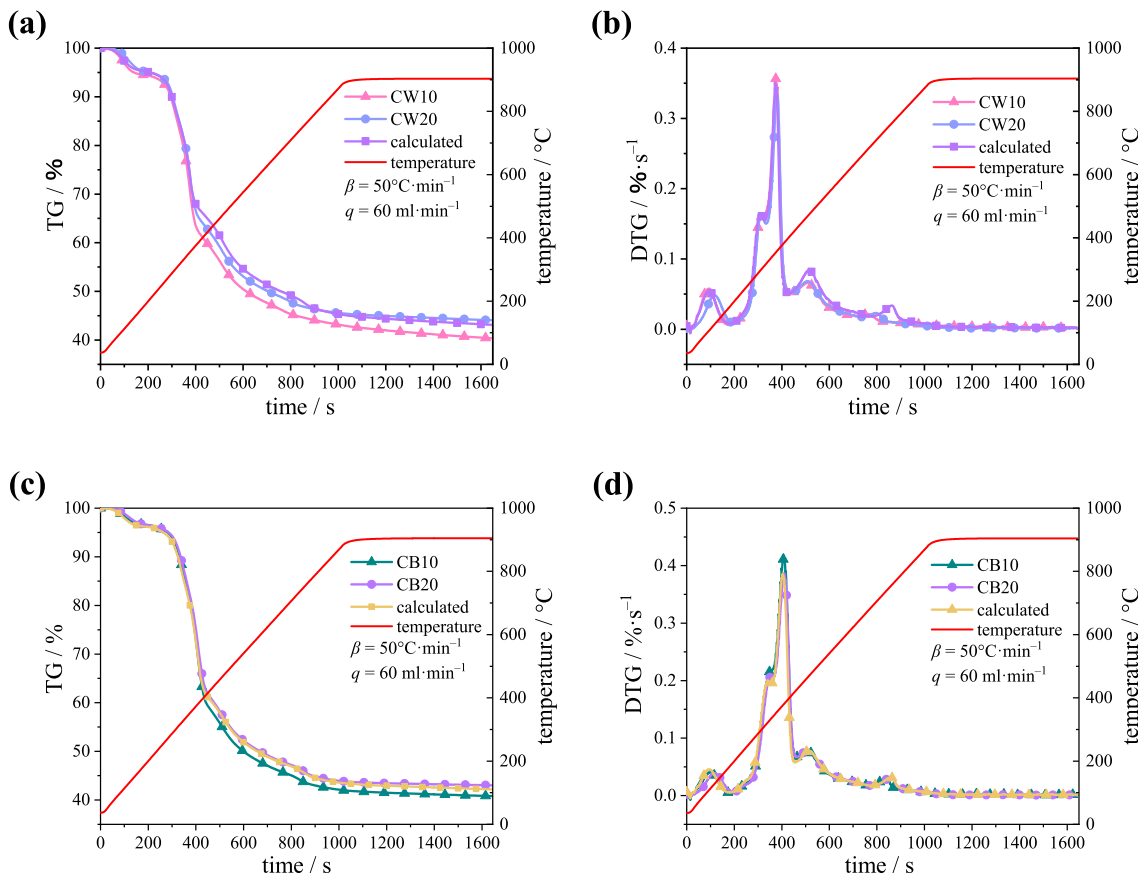


**Fig. 3** Co-pyrolysis curves based on the conventional thermogravimetric analysis method: **a** coal/wheat straw TG, **b** coal/wheat straw DTG, **c** coal/bamboo TG, and **d** coal/bamboo DTG

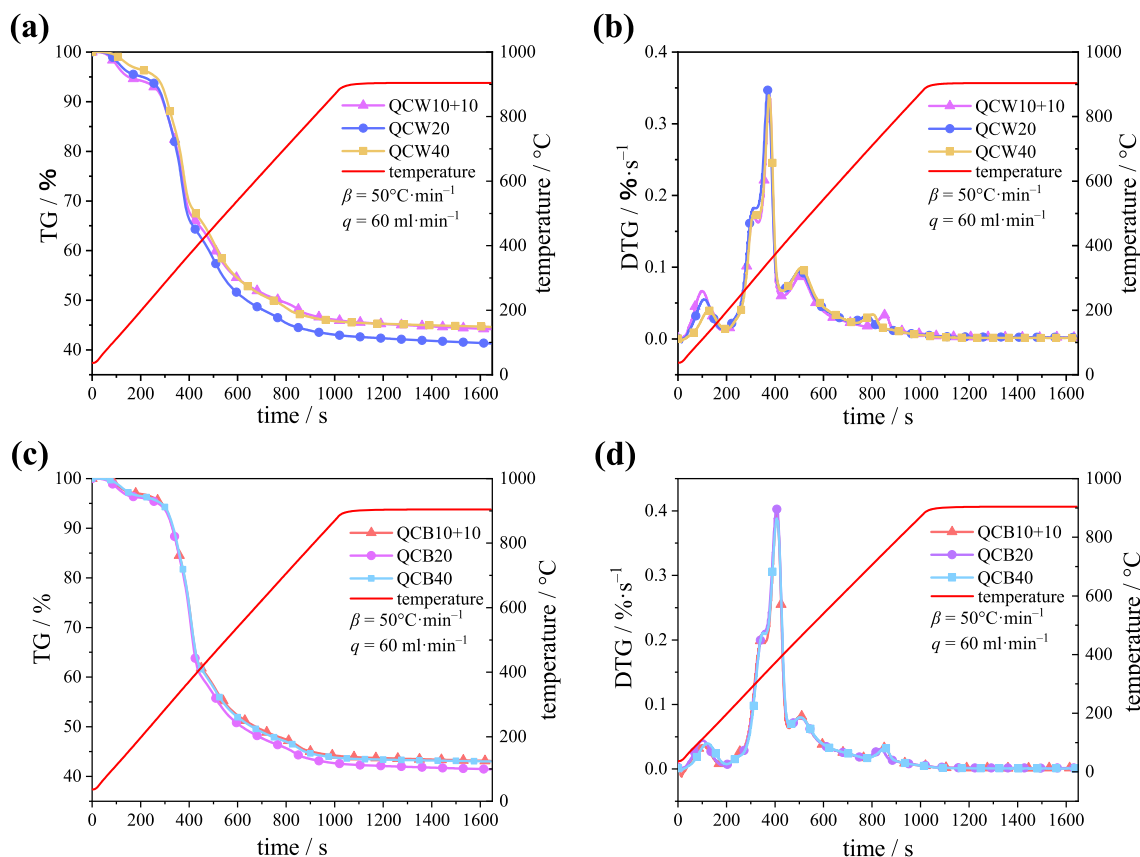


**Fig. 4** Co-pyrolysis curves based on the congruent–mass thermogravimetric analysis method: **a** coal/wheat straw TG, **b** coal/wheat straw DTG, **c** coal/bamboo TG, and **d** coal/bamboo DTG

coke yield of QCW20 after pyrolysis reaction is lower than that of QCW10+10. As seen from the DTG curves in Fig. 4b, the weight loss rate of the mixture (QCW20) during the pyrolysis process in the range of 200–500 °C is higher than that of the pyrolysis of the individual sample (QCW10+10). The DTG curve of QCW10+10 pyrolysis shows a weight loss peak (mainly the coking reaction of coal) at 720–800 °C, while the weight loss peak of DTG curve of QCW20 is significantly earlier than that of QCW10+10 pyrolysis. It is obvious that coal reacts more thoroughly in the primary pyrolysis regime, showing a significant synergistic effect during the co-pyrolysis of coal and wheat straw. Song et al. [38] have also found that the pyrolysis of biomass is the first step during the co-pyrolysis process, and H<sub>2</sub> released can be used as an external hydrogenation source for coal pyrolysis. Meanwhile, it is believed that the alkali metal ions contained in the volatiles can promote the decomposition of coal [39]. Chen et al. [40] found in their study that co-pyrolysis improved the yields of the hydrocarbon and phenol-type compounds and reduced the formations of the acid and nitrogenous compounds. As to the experimental runs QCB10+10 and QCB20, during co-pyrolysis of coal and bamboo, the TG curve of QCB20 in Fig. 4c is also lower than that of QCB10+10, and the relative quality difference  $\Delta M$  is greater than 0, and the RMS is 2.11. It

also indicates that the co-pyrolysis of coal and bamboo shows the synergistic effect to some extent.

Furthermore, it has been verified that the pyrolytic weight loss curve and the final coke yield of QCW40 and QCB40 are higher than those of QCW20 and QCB20, respectively. The RMS of relative quality difference  $\Delta M$  during the pyrolysis process at the different initial masses is 2.82 and 1.86, respectively. And then the coke yield increases with the increase of the initial sample mass.

Table 4 shows the main performance parameters during the pyrolysis process at different experimental runs. The volatiles release coefficients  $D_i$  of different samples during the main pyrolysis stage are calculated by the main parameters, to evaluate the reaction intensity and volatilization release degree in the main pyrolysis process. Figure 5 shows the variation tendency of volatiles release coefficients during pyrolysis and co-pyrolysis of coal, wheat straw, and bamboo. The main pyrolysis intervals  $D_i$  of wheat and bamboo were  $251.89 \times 10^{-9} \cdot \% \cdot s^{-1} \cdot ^\circ C^{-3}$  and  $127.35 \times 10^{-9} \cdot \% \cdot s^{-1} \cdot ^\circ C^{-3}$ , much higher than bituminous coal at  $6.82 \times 10^{-9} \cdot \% \cdot s^{-1} \cdot ^\circ C^{-3}$ , and the coal has a wider range of  $\Delta T_{1/2}$ , indicating that the reaction intensity of biomass is higher during pyrolysis, and volatiles are released significantly within the short time. Compared with biomass, the main pyrolysis duration of coal is longer. The temperature



**Table 4** Main characteristic parameters of pyrolysis and co-pyrolysis process

| Parameter                                                        | Coal                                                                                           | Wheat  | QCW10+10 | QCW20  | QCW40  | Bamboo | CB10+10 | QCB20  | QCB40  |  |
|------------------------------------------------------------------|------------------------------------------------------------------------------------------------|--------|----------|--------|--------|--------|---------|--------|--------|--|
|                                                                  | $\beta = 50 \text{ }^\circ\text{C}\cdot\text{min}^{-1}, q = 60 \text{ ml}\cdot\text{min}^{-1}$ |        |          |        |        |        |         |        |        |  |
| $T_b/^\circ\text{C}$                                             | 367.20                                                                                         | 201.87 | 201.64   | 201.84 | 202.33 | 200.01 | 210.13  | 215.21 | 212.82 |  |
| $T_{\max}/^\circ\text{C}$                                        | 474.26                                                                                         | 350.14 | 350.27   | 347.72 | 349.18 | 375.00 | 369.53  | 377.15 | 377.91 |  |
| $R_{\max}/\% \cdot \text{s}^{-1}$                                | 0.1291                                                                                         | 0.7266 | 0.3427   | 0.3508 | 0.3400 | 0.7542 | 0.3941  | 0.4106 | 0.3883 |  |
| $\Delta T_{1/2}/^\circ\text{C}$                                  | 108.66                                                                                         | 40.81  | 56.03    | 54.65  | 58.24  | 78.95  | 80.28   | 71.70  | 78.44  |  |
| $D_i/10^{-9}\cdot\% \cdot \text{s}^{-1}\cdot^\circ\text{C}^{-3}$ | 6.82                                                                                           | 251.89 | 86.65    | 91.45  | 82.62  | 127.35 | 63.22   | 70.56  | 61.56  |  |

that the maximum weight loss rate of bamboo reaches is slightly behind that of wheat straw.  $\Delta T_{1/2}$  of QCB20 run is greater than that of QCW20, while  $D_i$  of QCB20 is lower than that of QCW20, which is closely related to the difference physical properties of the two biomass samples. Furthermore,  $D_i$  of QCW20 and QCB20 are higher than those of QCW10+10 and QCB10+10, respectively, in the pyrolysis of coal and biomass by the congruent–mass thermogravimetric method. It further proves that under the condition that the total mass is equal to the mass of a single reactant, the mixed pyrolysis of coal and biomass releases a higher proportion of volatiles than the individual pyrolysis of the two samples. The range of mixed pyrolysis  $\Delta T_{1/2}$  is smaller, and the pyrolysis reaction is more intense; therefore, the synergy of biomass and coal during the pyrolysis process leads to a faster rate of release of volatiles.

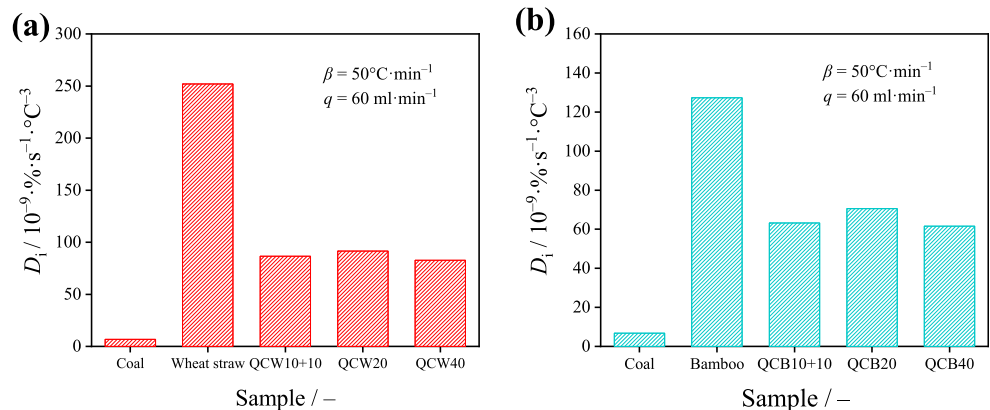
### 3.3 Influence of heating rate and carrier gas flow rate

Figure S1 shows the co-pyrolysis curves of mixture powders at different heating rates according to the congruent–mass thermogravimetric method. The overall tendency of pyrolysis of the same substance at different heating rates is basically the same, but there are certain differences during the pyrolysis process. As can be seen from the TG curves in Fig. S1 (a) and (c), the thermogravimetric curve presents certain hysteresis effect, and gradually shifts to the high temperature region as the heating rate rises. The high heating rate leads to the

strengthening of co-pyrolysis degree to some extent. According to the DTG curves illustrated in Fig. S1 (b) and (d), the temperatures corresponding to weightlessness peaks gradually move to the high temperature region when the heating rate rises.  $T_{\max}$  corresponding to maximum weight loss rate of QCW and QCB delays from 322 to 348  $^\circ\text{C}$ , and from 350 to 377  $^\circ\text{C}$ , respectively. The thermogravimetric curve of the main pyrolysis interval was shifted back by 20–40  $^\circ\text{C}$ . The weight loss rate at high heating rate is significantly higher than that at low heating rate. Compared with 10  $^\circ\text{C}\cdot\text{min}^{-1}$ , the final coke yield of QCW at 30  $^\circ\text{C}\cdot\text{min}^{-1}$  and 50  $^\circ\text{C}\cdot\text{min}^{-1}$  decreased by 0.48% and 1.56%, respectively, and the final coke yield of QCB decreased by 0.36% and 0.96% respectively.

Figure S2 shows the co-pyrolysis curves of coal and biomass at different carrier gas flow rates according to the congruent–mass thermogravimetric method. As seen from Fig. S2 (a) and (c), the carrier gas flow rate also has the influence on the co-pyrolysis of coal and biomass. As the carrier gas flow rate rises, the final coke yield of QCW increased by 1.54% and 2.46%, and the final coke yield of QCB increased by 0.72% and 1.95%, respectively, and the synergistic effect of co-pyrolysis of mixture powders weakens. Volatile substances released in the pyrolysis process may be directly taken out under the condition of large carrier gas flow rate, which will affect the synergistic effect. In the DTG curves of Fig. S2 (b) and (d), the maximum pyrolysis weight loss rate with small carrier gas flow rate is slightly higher than that with large

**Fig. 5** Variation tendency of volatile component release coefficient: **a** coal/wheat straw and **b** coal/bamboo



carrier gas flow rate, which proves that the synergistic effect of co-pyrolysis of coal and biomass is affected with the increase of carrier gas flow rate.

The main characteristic parameters of pyrolysis process at different heating rates and carrier gas flows rates are listed in Table S1. Figure 6 shows the variation tendency of volatiles release coefficients in the main pyrolysis intervals at different heating rates and carrier gas flow rates. As the heating rate rises, the maximum pyrolysis weight loss rate  $R_{\max}$  increases, and the temperature corresponding to the maximum weight loss rate delays to the high temperature region.  $\Delta T_{1/2}$  grows bigger with a wider thermal decomposition weightlessness peak. The volatiles release coefficient increased significantly in unit time, and the main pyrolysis intervals  $D_i$  of wheat straw increased from  $23.62 \times 10^{-9}$  to  $92.59 \times 10^{-9} \cdot \% \cdot s^{-1} \cdot ^\circ C^{-3}$ , and that of bamboo increased from  $26.76 \times 10^{-9}$  to  $68.48 \times 10^{-9} \cdot \% \cdot s^{-1} \cdot ^\circ C^{-3}$ , indicating that the reaction was more intense in unit time at high heating rate. Huang et al. [41] reached a similar conclusion in the pyrolysis study of water hyacinth roots, stems, and leaves; the elevated heating rate raised both initial devolatilization and peak temperatures and shortened the reaction times of the thermochemical conversions of both samples. As the carrier gas flow rate rises, the maximum weight loss rate  $R_{\max}$  of coal and biomass mixture decreases, and the volatiles release coefficient decreases. The main pyrolysis intervals  $D_i$  of wheat straw decreased from  $92.59 \times 10^{-9}$  to  $60.5 \times 10^{-9} \cdot \% \cdot s^{-1} \cdot ^\circ C^{-3}$ , and that of bamboo decreased from  $68.48 \times 10^{-9}$  to  $62.47 \times 10^{-9} \cdot \% \cdot s^{-1} \cdot ^\circ C^{-3}$ . The synergistic effect of coal and biomass co-pyrolysis weakens at high carrier gas flow rate. The influence of heating rate and carrier gas flow rate on the co-pyrolysis of coal and wheat straw is more significant than that of coal and bamboo.

### 3.4 Kinetic analysis of pyrolysis processes

Table 5 shows the kinetic parameters of the main pyrolysis temperature range of the samples when the congruent–mass thermogravimetric method is adopted. The calculated conversion rates  $\alpha_c$  of samples show a good agreement with the

experimental conversion rate  $\alpha$  of samples. Usually, the lower the activation energy is, the easier the reaction is to achieve [42]. Lowering the activation energy will effectively promote the reaction. The Coats–Redfern method was used to calculate the pyrolysis kinetic parameters of coal and biomass. It was found that the pyrolysis of coal and biomass was a complex reaction process, involving several first-order and multistage reactions. The higher the activation energy, the higher the pre-exponential factor. It can be seen from the data that the main pyrolysis temperature range of Wheat and Bamboo is about 320–375 °C and 340–400 °C, and the main pyrolysis temperature range of coal is about 440–540 °C. The activation energy in the main pyrolysis reaction stage of wheat straw and bamboo is  $692.40 \text{ kJ} \cdot \text{mol}^{-1}$  and  $683.73 \text{ kJ} \cdot \text{mol}^{-1}$ , respectively, which is much higher than that coal ( $343.07 \text{ kJ} \cdot \text{mol}^{-1}$ ). It indicates that the main pyrolysis temperature range of biomass is narrower, and strong decomposition occurs in a short period of time. At the same time, a large amount of energy is needed. Compared with biomass, coal pyrolysis is slower. By comparing the activation energy of pyrolysis of coal and biomass, and their mixture obtained by the congruent–mass thermogravimetric analysis method with those of separate pyrolysis of coal or biomass, it is found that the  $E$  required for QCW20 run is  $432.38 \text{ kJ} \cdot \text{mol}^{-1}$  in the range of 348.59–385.54 °C, which is lower than  $457.52 \text{ kJ} \cdot \text{mol}^{-1}$  for QCW10+10 run. In the range of 400–560 °C coal pyrolysis temperature, the  $E$  of QCW20 run is lower than that of QCW10+10 run. It indicates that the co-pyrolysis of coal and wheat straw is easier than the separate reaction within the main pyrolysis temperature range. The volatiles produced by biomass pyrolysis promote the pyrolysis of coal. As to the co-pyrolysis experiment of coal and bamboo, it is found that the activation energy of QCB20 run in the range of 378.00–410.51 °C is  $504.63 \text{ kJ} \cdot \text{mol}^{-1}$ , which is lower than the  $520.68 \text{ kJ} \cdot \text{mol}^{-1}$  of QCB10+10 run. The activation energy of QCB20 is also lower than that of QCB10+10 in the temperature range of 416–458 °C; the potential synergistic effect occurs in the co-pyrolysis process of coal and bamboo. The verification of QCW40 and QCB40 further proves that with the increase of reactant initial mass, the

**Fig. 6** Variation tendency of volatiles release coefficients in the main pyrolysis intervals at different heating rates and carrier gas flow rates: **a** different heating rates and **b** different carrier gas flow rates

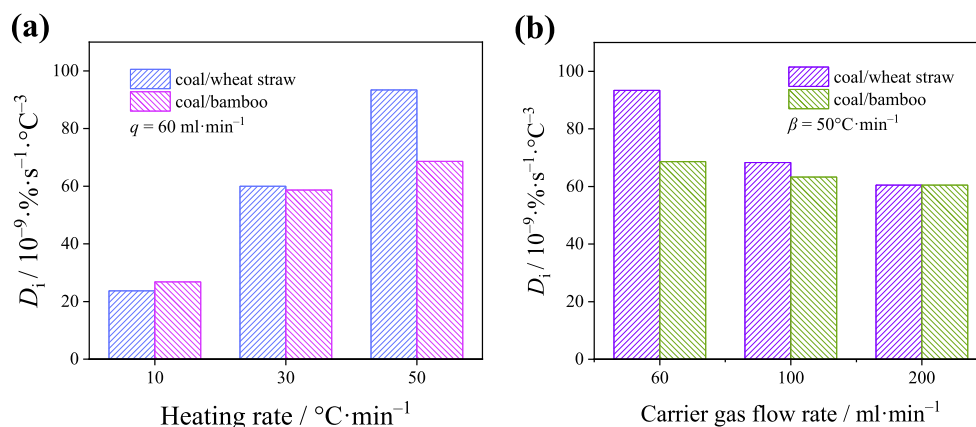


**Table 5** Kinetic parameters of coal and biomass pyrolysis process

| $T/^\circ\text{C}$                                                                                            | $E/\text{kJ}\cdot\text{mol}^{-1}$ | $A/\text{s}^{-1}$   | $f(\alpha)$        | $R^2$  | $T/^\circ\text{C}$ | $E/\text{kJ}\cdot\text{mol}^{-1}$ | $A/\text{s}^{-1}$    | $f(\alpha)$        | $R^2$  |
|---------------------------------------------------------------------------------------------------------------|-----------------------------------|---------------------|--------------------|--------|--------------------|-----------------------------------|----------------------|--------------------|--------|
| Pyrolysis, $\beta = 50\text{ }^\circ\text{C}\cdot\text{min}^{-1}$ , $q = 60\text{ ml}\cdot\text{min}^{-1}$    |                                   |                     |                    |        |                    |                                   |                      |                    |        |
| Coal                                                                                                          |                                   |                     |                    |        | Wheat              |                                   |                      |                    |        |
| 441.19–474.26                                                                                                 | 469.3                             | $1.64\text{E} + 32$ | $(1-\alpha)$       | 0.9918 | 251.39–320.34      | 198.81                            | $1.09\text{E} + 11$  | $(1-\alpha)^{1.5}$ | 0.9910 |
| 475.10–540.54                                                                                                 | 343.07                            | $6.49\text{E} + 21$ | $(1-\alpha)^{1.8}$ | 0.9904 | 321.22–350.14      | 432.21                            | $7.94\text{E} + 35$  | $(1-\alpha)^{1.5}$ | 0.9954 |
| 561.39–680.36                                                                                                 | 215.44                            | $1.04\text{E} + 11$ | $(1-\alpha)^{1.5}$ | 0.9860 | 351.01–375.34      | 692.40                            | $2.06\text{E} + 56$  | $(1-\alpha)^{1.8}$ | 0.9940 |
| 696.12–763.47                                                                                                 | 438.95                            | $1.53\text{E} + 21$ | $(1-\alpha)$       | 0.9906 | 376.19–520.89      | 109.34                            | $2.36\text{E} + 6$   | $(1-\alpha)^{1.5}$ | 0.9854 |
| Bamboo                                                                                                        |                                   |                     |                    |        |                    |                                   |                      |                    |        |
| 271.33–340.70                                                                                                 | 208.21                            | $1.67\text{E} + 17$ | $(1-\alpha)^{1.5}$ | 0.9893 |                    |                                   |                      |                    |        |
| 341.56–375.86                                                                                                 | 393.31                            | $1.88\text{E} + 31$ | $(1-\alpha)^{1.5}$ | 0.9954 |                    |                                   |                      |                    |        |
| 376.71–400.58                                                                                                 | 683.73                            | $1.87\text{E} + 53$ | $(1-\alpha)^{1.6}$ | 0.9913 |                    |                                   |                      |                    |        |
| 401.43–560.11                                                                                                 | 91.28                             | $5.61\text{E} + 4$  | $(1-\alpha)^{1.4}$ | 0.9841 |                    |                                   |                      |                    |        |
| Co-pyrolysis, $\beta = 50\text{ }^\circ\text{C}\cdot\text{min}^{-1}$ , $q = 60\text{ ml}\cdot\text{min}^{-1}$ |                                   |                     |                    |        |                    |                                   |                      |                    |        |
| QCW10+10                                                                                                      |                                   |                     |                    |        | QCW20              |                                   |                      |                    |        |
| 231.34–303.23                                                                                                 | 154.02                            | $1.17\text{E} + 13$ | $(1-\alpha)$       | 0.9906 | 225.44–298.13      | 148.29                            | $4.29\text{E} + 12$  | $(1-\alpha)$       | 0.9894 |
| 304.10–350.25                                                                                                 | 216.27                            | $1.9\text{E} + 17$  | $(1-\alpha)$       | 0.9887 | 299.87–347.72      | 209.59                            | $6.27\text{E} + 16$  | $(1-\alpha)$       | 0.9987 |
| 351.14–386.42                                                                                                 | 457.52                            | $5.11\text{E} + 36$ | $(1-\alpha)^{1.9}$ | 0.9907 | 348.59–385.54      | 432.38                            | $4.89\text{E} + 34$  | $(1-\alpha)^{1.9}$ | 0.9905 |
| 401.78–462.69                                                                                                 | 235.42                            | $7.47\text{E} + 15$ | $(1-\alpha)$       | 0.9857 | 400.04–461.81      | 227.08                            | $1.8\text{E} + 15$   | $(1-\alpha)$       | 0.9864 |
| 463.53–560.28                                                                                                 | 230.78                            | $1.31\text{E} + 14$ | $(1-\alpha)^{1.8}$ | 0.9849 | 462.65–560.48      | 227.11                            | $17.43\text{E} + 13$ | $(1-\alpha)^{1.8}$ | 0.9848 |
| QCW40                                                                                                         |                                   |                     |                    |        | QCB10+10           |                                   |                      |                    |        |
| 225.85–299.51                                                                                                 | 145.87                            | $2.12\text{E} + 12$ | $(1-\alpha)$       | 0.9875 | 256.37–325.42      | 176.95                            | $3.77\text{E} + 14$  | $(1-\alpha)$       | 0.9902 |
| 300.25–349.18                                                                                                 | 211.47                            | $8.45\text{E} + 16$ | $(1-\alpha)$       | 0.9829 | 327.17–369.54      | 254.43                            | $8.24\text{E} + 19$  | $(1-\alpha)$       | 0.9847 |
| 350.05–385.33                                                                                                 | 438.34                            | $1.15\text{E} + 35$ | $(1-\alpha)^{1.9}$ | 0.9861 | 370.40–402.13      | 520.68                            | $2.69\text{E} + 40$  | $(1-\alpha)^{1.6}$ | 0.9916 |
| 400.66–461.59                                                                                                 | 234.83                            | $6.8\text{E} + 15$  | $(1-\alpha)$       | 0.9857 | 420.01–462.23      | 347.94                            | $1.09\text{E} + 24$  | $(1-\alpha)$       | 0.9856 |
| 462.43–560.14                                                                                                 | 228.39                            | $9.23\text{E} + 13$ | $(1-\alpha)^{1.8}$ | 0.9849 | 463.07–563.11      | 231.51                            | $1.55\text{E} + 14$  | $(1-\alpha)^2$     | 0.9903 |
| QCB20                                                                                                         |                                   |                     |                    |        | QCB40              |                                   |                      |                    |        |
| 263.31–332.26                                                                                                 | 178.53                            | $3.47\text{E} + 14$ | $(1-\alpha)$       | 0.9931 | 264.49–333.73      | 182.28                            | $3.9\text{E} + 14$   | $(1-\alpha)$       | 0.9939 |
| 333.13–377.15                                                                                                 | 257.52                            | $8.17\text{E} + 19$ | $(1-\alpha)$       | 0.9911 | 334.61–377.92      | 261.83                            | $1.74\text{E} + 20$  | $(1-\alpha)$       | 0.9915 |
| 378.00–410.51                                                                                                 | 504.63                            | $6.1\text{E} + 38$  | $(1-\alpha)^{1.6}$ | 0.9944 | 378.78–410.50      | 532.52                            | $1.7\text{E} + 40$   | $(1-\alpha)^{1.6}$ | 0.9906 |
| 416.47–458.76                                                                                                 | 334.67                            | $1.58\text{E} + 23$ | $(1-\alpha)$       | 0.9852 | 416.47–458.82      | 333.56                            | $1.3\text{E} + 23$   | $(1-\alpha)$       | 0.9853 |
| 459.60–559.69                                                                                                 | 218.45                            | $1.99\text{E} + 13$ | $(1-\alpha)^{1.8}$ | 0.9874 | 459.67–559.79      | 219.03                            | $2.21\text{E} + 13$  | $(1-\alpha)^{1.8}$ | 0.9877 |

activation energy needed for the thermal degradation process increases gradually.

The kinetic parameters of the main co-pyrolysis process at different heating rates and carrier gas flow rates are listed in Table S2. As the heating rate increases, the  $E$  needed for the co-pyrolysis of mixture powders shows an increasing trend in the main pyrolysis interval, which proves that the interaction between coal and biomass is more intense and consumes more energy at the high heating rate. While as the carrier gas flow rate increases, the  $E$  needed for co-pyrolysis increases, and the synergistic effect of interaction of coal and biomass weakens.

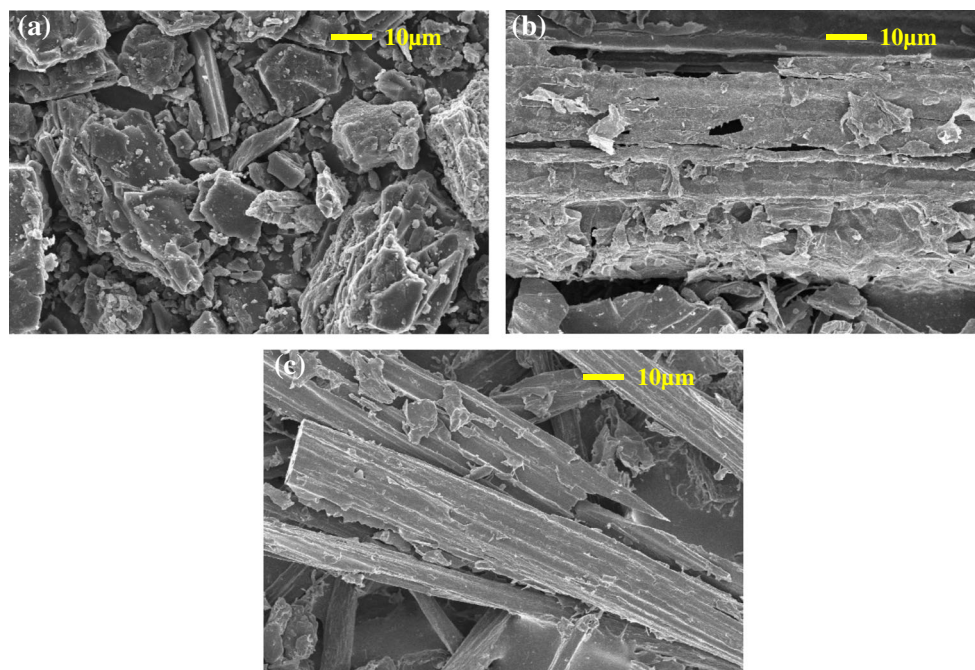
### 3.5 Coke morphology analysis

Figure 7 illustrates the SEM images of coke products of bituminous coal and biomass pyrolysis. It is obvious that the cokes produced by bituminous coal, wheat straw, and bamboo

have different surface morphologies. As shown in Fig. 7a, the coke of bituminous coal is mainly composed of a large number of granular substances with relatively smooth surface and few pores. Biomass coke has an extremely irregular shape, with a more complex pore structure and a larger specific surface area. Wheat straw coke is mainly in irregular rod shaped and block shaped, with well-developed pore structure, uneven particle surface, and a large number of collapses, while bamboo coke products show the smaller overall, mostly slender rod-shaped structure, with irregular folded pits on the surface. The complex pore structure of biomass coke is conducive to the release of volatiles, promoting the strong adsorption characteristics for the powders.

As to the coke products obtained by co-pyrolysis of coal and biomass, quite different morphological characteristics are observed. During the co-pyrolysis process, the fine particles of the coal are fully adsorbed on the surface of biomass coke, and in

**Fig. 7** SEM micrographs of individual pyrolysis produced cokes with the heating rate of  $\beta = 50 \text{ }^\circ\text{C}\cdot\text{min}^{-1}$  and the carrier gas flow rate of  $q = 60 \text{ ml}\cdot\text{min}^{-1}$ : **a** coal, **b** wheat straw, and **c** bamboo



close contact with the volatiles, which can be clearly seen that a large amount of coal particles are attached to the surface of biomass coke. Figure 8 illustrates the SEM images of co-pyrolysis process coke products of bituminous coal and biomass pyrolysis obtained by the congruent–mass thermogravimetric method. Figure 8a–d also show that the co-pyrolysis coke has more developed surface pores and more fine particles are produced. Figures S3 and S4 show the SEM patterns of co-pyrolysis produced cokes at different heating rates and

different carrier gas flow rates. The box dimension can reflect the irregular degree of coke structure. The more abundant the pores of coke, the greater degree of irregularity on the surface, and the greater the fractal dimension of the coke [43]. Wu et al. [44] have suggested that the surface morphology of co-pyrolysis coke of coal and microalgae changed from dense phase to loose accumulation, with obvious porous structure, and the fractal dimension of coke is between 1.43 and 1.82. Zhang et al. [45] found in the co-pyrolysis study of textile

**Fig. 8** SEM micrographs of co-pyrolysis produced cokes by the congruent–mass thermogravimetric method with the heating rate of  $\beta = 50 \text{ }^\circ\text{C}\cdot\text{min}^{-1}$  and the carrier gas flow rate of  $q = 60 \text{ ml}\cdot\text{min}^{-1}$ : **a** QCW20, **b** QCW40, **c** QCB20, and **d** QCB 40

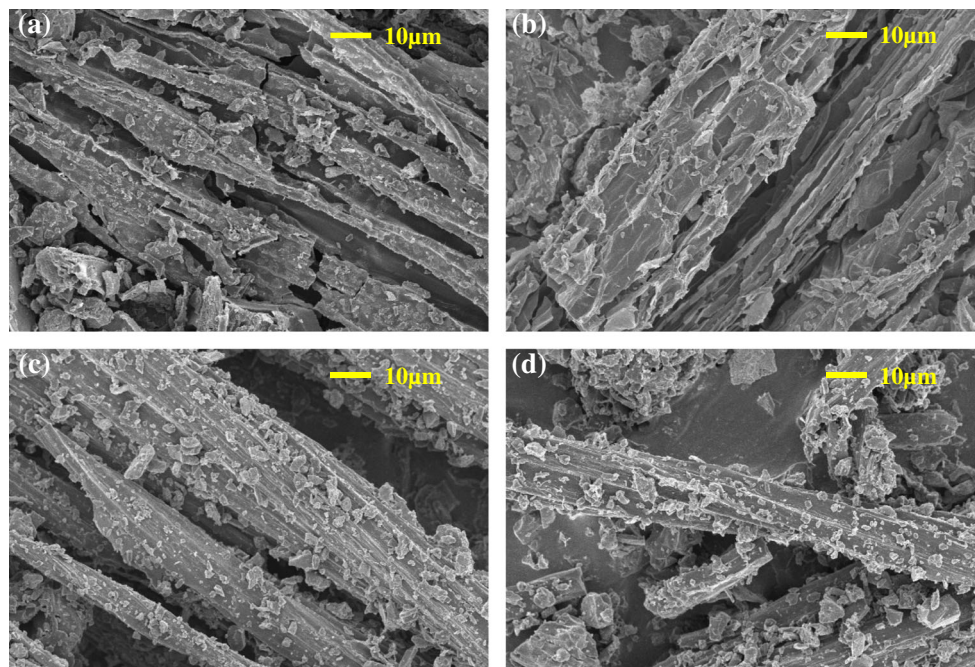


**Table 6** The fractal dimension of coke products

| Parameters | Coal<br>$\beta = 50 \text{ }^\circ\text{C}\cdot\text{min}^{-1}, q = 60 \text{ ml}\cdot\text{min}^{-1}$ | Wheat  | Bamboo | QCW20  | QCW40  | QCB20  | QCB40  |
|------------|--------------------------------------------------------------------------------------------------------|--------|--------|--------|--------|--------|--------|
| $D_s$      | 1.4259                                                                                                 | 1.5371 | 1.4288 | 1.6292 | 1.6269 | 1.5261 | 1.5364 |
| $R^2$      | 0.9957                                                                                                 | 0.9942 | 0.9905 | 0.9912 | 0.9951 | 0.9916 | 0.9921 |

**Table 7** The fractal dimension of coke products at different heating rates and carrier gas flow rates

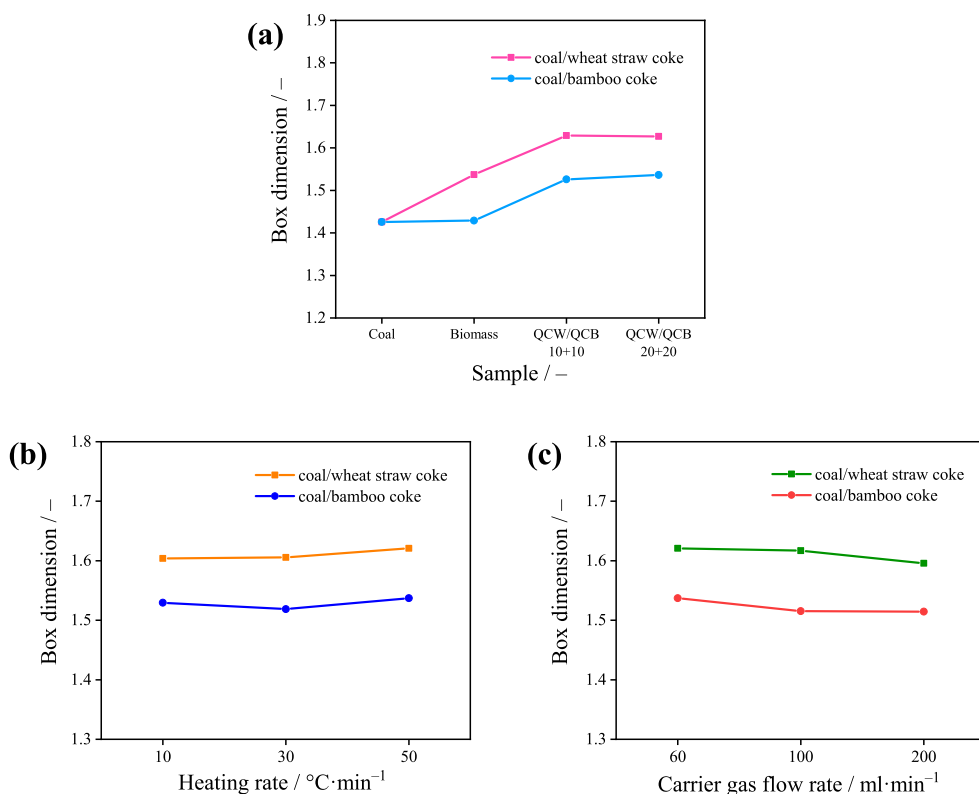
| Parameters | QCW10 ( $q = 60 \text{ ml}\cdot\text{min}^{-1}$ )                 |        |        | QCB10 ( $q = 60 \text{ ml}\cdot\text{min}^{-1}$ )                 |        |        |        |
|------------|-------------------------------------------------------------------|--------|--------|-------------------------------------------------------------------|--------|--------|--------|
|            | $\beta/^\circ\text{C}\cdot\text{min}^{-1}$                        | 10     | 30     | 50                                                                | 10     | 30     | 50     |
| $D_s$      |                                                                   | 1.6038 | 1.6055 | 1.6210                                                            | 1.5296 | 1.5188 | 1.5370 |
| $R^2$      |                                                                   | 0.9923 | 0.9926 | 0.9909                                                            | 0.9963 | 0.9933 | 0.9946 |
| Parameters | QCW10 ( $\beta = 50 \text{ }^\circ\text{C}\cdot\text{min}^{-1}$ ) |        |        | QCB10 ( $\beta = 50 \text{ }^\circ\text{C}\cdot\text{min}^{-1}$ ) |        |        |        |
|            | $q/\text{ml}\cdot\text{min}^{-1}$                                 | 60     | 100    | 200                                                               | 60     | 100    | 200    |
| $D_s$      |                                                                   | 1.6210 | 1.6169 | 1.5958                                                            | 1.5370 | 1.5154 | 1.5146 |
| $R^2$      |                                                                   | 0.9909 | 0.9945 | 0.9910                                                            | 0.9946 | 0.9947 | 0.9903 |

dyeing sludge (TDS) and cattle manure (CM) that co-pyrolytic char had a longer aliphatic chain length and higher aromaticity than did the mono-pyrolytic chars.

Table 6 and Table 7 list the box dimension of cokes according to the fractal geometry, and the variation tendency chart of box dimension of cokes is illustrated in Fig. 9. The

results show that the box dimension of cokes is between 1.4259 and 1.6398, and the box dimension of wheat straw ( $D_s = 1.5371$ ) and bamboo ( $D_s = 1.4288$ ) is greater than that of bituminous coal ( $D_s = 1.4259$ ), further indicating that biomass coke has a more developed pore structure. The box dimension of coke obtained by co-pyrolysis of mixture powders

**Fig. 9** Variation tendency chart of box dimension of cokes produced by the congruent-mass thermogravimetric analysis method: **a** box dimension of pyrolysis and co-pyrolysis cokes, **b** box dimension of cokes at different heating rates, and **c** box dimension of cokes with different carrier gas flow rates



is also higher than that obtained by pyrolysis of individual samples (coal and wheat straw).

The interaction between the two compounds during the co-pyrolysis process has the significant effect on the properties of produced cokes, which makes the micropores on the coke surface diffuse and forms a more developed pore structure, further improving the overall porosity characteristic of cokes. It confirms that the co-pyrolysis of the mixture of coal and biomass powders has the high activity and positive synergy effect. The box dimension of low heating rate pyrolysis coke is slightly smaller than that of high heating rate pyrolysis coke. With the increase of flow rate of carrier gas, the box dimension of coke surface decreases; it is deemed that the flow rate of carrier gas has a certain influence on the synergistic effect of co-pyrolysis as discussed earlier.

## 4 Conclusions

In this study, two different thermogravimetric analysis strategies (conventional thermogravimetric method and congruent–mass thermogravimetric method) were conducted to study the potential interaction mechanisms of coal and biomass co-pyrolysis process. The effects of heating rate and carrier gas flow rate on co-pyrolysis were investigated. The kinetics of the main thermal reaction stages and surface morphologies of pyrolysis products are also analyzed. The main conclusions are as follows:

- 1) The influence of initial sample mass on the determination of interaction of the mixed samples can be reduced by using the congruent–mass thermogravimetric analysis method. The method can also compare the interactions in the co-pyrolysis process more intuitively. The pyrolysis TG curve of QCW20 and QCW20 and is significantly lower than that of QCW10+10 and QCW10+10, respectively, and the relative quality difference  $\Delta M$  is greater than 0. The main pyrolysis intervals  $D_i$  of mixtures are higher than that of the individual pyrolysis. The co-pyrolysis of mixture powders shows a synergistic effect.
- 2) As the heating rate rises, the TG curve of co-pyrolysis of coal and biomass shows a certain hysteresis, and the weight loss peak gradually shifts to the high temperature region. While as the carrier gas flow rate rises, the yield of co-pyrolysis coke increases, and the synergistic effect of two components in the co-pyrolysis weakens.
- 3) The co-pyrolysis reaction is easier than the separate reaction within the main pyrolysis temperature regime. As the reactant mass increases, the  $E$  needed for the degradation process increases gradually. Co-pyrolysis reactions require higher activation energy at a high heating rate or with a large carrier gas flow rate.
- 4) Biomass coke is more uneven than coal and has higher fractal dimension. The box dimension of coke obtained by co-pyrolysis of mixture powders is also higher than that of individual samples. The interaction between the two components during co-pyrolysis process forms a much more developed pore structure, and increases the overall porosity characteristic of coke.

**Supplementary Information** The online version contains supplementary material available at <https://doi.org/10.1007/s13399-021-01502-0>.

**Funding** This work was financially supported by the Fundamental Research Funds for the Central Universities (DUT20LAB134).

## Declarations

**Conflict of interest** The authors declare no competing interests.

## References

1. Wang K, Tong Y, Yue T, Gao J, Wang C, Zuo P, Liu J (2021) Measure-specific environmental benefits of air pollution control for coal-fired industrial boilers in China from 2015 to 2017. *Environ Pollut* 273:116470. <https://doi.org/10.1016/j.envpol.2021.116470>
2. Mohsin M, Kamran HW, Atif Nawaz M, Sajjad Hussain M, Dahri AS (2021) Assessing the impact of transition from nonrenewable to renewable energy consumption on economic growth–environmental nexus from developing Asian economies. *J Environ Manag* 284:111999. <https://doi.org/10.1016/j.jenvman.2021.111999>
3. Muigai HH, Choudhury BJ, Kalita P, Moholkar VS (2020) Co-pyrolysis of biomass blends: characterization, kinetic and thermodynamic analysis. *Biomass Bioenergy* 143:105839. <https://doi.org/10.1016/j.biombioe.2020.105839>
4. Vassilev SV, Baxter D, Andersen LK, Vassileva CG (2010) An overview of the chemical composition of biomass. *Fuel* 89(5): 913–933. <https://doi.org/10.1016/j.fuel.2009.10.022>
5. Rusch F, Wastowski AD, de Lira TS, Moreira KCCS, de Moraes LD (2021) Description of the component properties of species of bamboo: a review. *Biomass Convers Bior.* <https://doi.org/10.1007/s13399-021-01359-3>
6. Yang Z, Wu Y, Zhang Z, Li H, Li X, Egorov RI, Strizhak PA, Gao X (2019) Recent advances in co-thermochemical conversions of biomass with fossil fuels focusing on the synergistic effects. *Renew Sust Energ Rev* 103:384–398. <https://doi.org/10.1016/j.rser.2018.12.047>
7. Agarwal G, Lattimer B (2014) Physicochemical, kinetic and energetic investigation of coal–biomass mixture pyrolysis. *Fuel Process Technol* 124:174–187. <https://doi.org/10.1016/j.fuproc.2014.03.005>
8. Khan SR, Zeeshan M, Khokhar MF, Zeshan AI (2021) A comprehensive study on upgradation of pyrolysis products through co-feeding of waste tire into rice straw under broad range of co-feed ratios in a bench-scale fixed bed reactor. *Biomass Convers Bior.* <https://doi.org/10.1007/s13399-021-01434-9>
9. Mu L, Chen J, Yao P, Zhou D, Zhao L, Yin H (2016) Evaluation of co-pyrolysis petrochemical wastewater sludge with lignite in a thermogravimetric analyzer and a packed-bed reactor: pyrolysis characteristics, kinetics, and products analysis. *Bioresour Technol* 221:147–156. <https://doi.org/10.1016/j.biortech.2016.09.011>

10. Muthuraman M, Namioka T, Yoshikawa K (2010) A comparative study on co-combustion performance of municipal solid waste and Indonesian coal with high ash Indian coal: a thermogravimetric analysis. *Fuel Process Technol* 91(5):550–558. <https://doi.org/10.1016/j.fuproc.2009.12.018>
11. Chen C, Ma X, He Y (2012) Co-pyrolysis characteristics of microalgae *Chlorella vulgaris* and coal through TGA. *Bioresour Technol* 117:264–273. <https://doi.org/10.1016/j.biortech.2012.04.077>
12. Chen J, Wang Y, Lang X, Ren X, Fan S (2017) Evaluation of agricultural residues pyrolysis under non-isothermal conditions: thermal behaviors, kinetics, and thermodynamics. *Bioresour Technol* 241:340–348. <https://doi.org/10.1016/j.biortech.2017.05.036>
13. Cordero T, Rodriguez Mirasol J, Pastrana J, Rodriguez JJ (2004) Improved solid fuels from co-pyrolysis of a high-sulphur content coal and different lignocellulosic wastes. *Fuel* 83(11–12):1585–1590. <https://doi.org/10.1016/j.fuel.2004.02.013>
14. Hu Z, Ma X, Li L (2016) The synergistic effect of co-pyrolysis of oil shale and microalgae to produce syngas. *J Energy Inst* 89(3):447–455. <https://doi.org/10.1016/j.joei.2015.02.009>
15. Kumar M, Srivastava N, Upadhyay SN, Mishra PK (2021) Thermal degradation of dry kitchen waste: kinetics and pyrolysis products. *Biomass Convers Bior.* <https://doi.org/10.1007/s13399-021-01309-z>
16. Masnadi MS, Habibi R, Kopyscinski J, Hill JM, Bi X, Lim CJ, Ellis N, Grace JR (2014) Fuel characterization and co-pyrolysis kinetics of biomass and fossil fuels. *Fuel* 117:1204–1214. <https://doi.org/10.1016/j.fuel.2013.02.006>
17. Mu L, Zhao C, Zhao L, Chen B, Xu Z, Yang Z, Shang Y, Yin H (2018) Mineralogical composition evolution and thermogravimetric characteristics of sewage sludge ash at different ashing temperatures. *Energy Fuel* 32(12):12617–12629. <https://doi.org/10.1021/acs.energyfuels.8b03384>
18. Sadhukhan AK, Gupta P, Goyal T, Saha RK (2008) Modelling of pyrolysis of coal-biomass blends using thermogravimetric analysis. *Bioresour Technol* 99(17):8022–8026. <https://doi.org/10.1016/j.biortech.2008.03.047>
19. Park DK, Kim SD, Lee SH, Lee JG (2010) Co-pyrolysis characteristics of sawdust and coal blend in TGA and a fixed bed reactor. *Bioresour Technol* 101(15):6151–6156. <https://doi.org/10.1016/j.biortech.2010.02.087>
20. Aboyade AO, Görgens JF, Carrier M, Meyer EL, Knoetze JH (2013) Thermogravimetric study of the pyrolysis characteristics and kinetics of coal blends with corn and sugarcane residues. *Fuel Process Technol* 106:310–320. <https://doi.org/10.1016/j.fuproc.2012.08.014>
21. Wen S, Zou H, Liu J, Evrendilek DE, Yan Y, Liang G (2021) Multi-response optimization toward efficient and clean (co-)combustions of textile dyeing sludge and second-generation feedstock. *J Hazard Mater* 408:124824. <https://doi.org/10.1016/j.jhazmat.2020.124824>
22. Idris SS, Rahman NA, Ismail K, Alias AB, Rashid ZA, Aris MJ (2010) Investigation on thermochemical behaviour of low rank Malaysian coal, oil palm biomass and their blends during pyrolysis via thermogravimetric analysis (TGA). *Bioresour Technol* 101(12):4584–4592. <https://doi.org/10.1016/j.biortech.2010.01.059>
23. Vhathvarothai N, Ness J, Yu QJ (2014) An investigation of thermal behaviour of biomass and coal during copyrolysis using thermogravimetric analysis. *Int J Energy Res* 38(9):1145–1154. <https://doi.org/10.1002/er.3120>
24. Zhang Y, Fan D, Zheng Y (2016) Comparative study on combined co-pyrolysis/gasification of walnut shell and bituminous coal by conventional and congruent-mass thermogravimetric analysis (TGA) methods. *Bioresour Technol* 199:382–385. <https://doi.org/10.1016/j.biortech.2015.07.120>
25. Du Y, Jiang X, Lv G, Ma X, Jin Y, Wang F, Chi Y, Yan J (2014) Thermal behavior and kinetics of bio-ferment residue/coal blends during co-pyrolysis. *Energ Convers Manage* 88:459–463. <https://doi.org/10.1016/j.enconman.2014.08.068>
26. Sonobe T, Worasuwannarak N, Pipatmanomai S (2008) Synergies in co-pyrolysis of Thai lignite and comcob. *Fuel Process Technol* 89(12):1371–1378. <https://doi.org/10.1016/j.fuproc.2008.06.006>
27. Wu Z, Wang S, Zhao J, Chen L, Meng H (2016) Thermochemical behavior and char morphology analysis of blended bituminous coal and lignocellulosic biomass model compound co-pyrolysis: effects of cellulose and carboxymethylcellulose sodium. *Fuel* 171:65–73. <https://doi.org/10.1016/j.fuel.2015.12.057>
28. Rathore NS, Pawar A, Panwar NL (2021) Kinetic analysis and thermal degradation study on wheat straw and its biochar from vacuum pyrolysis under non-isothermal condition. *Biomass Convers Bior.* <https://doi.org/10.1007/s13399-021-01360-w>
29. Tong W, Cai Z, Liu Q, Ren S, Kong M (2020) Effect of pyrolysis temperature on bamboo char combustion: reactivity, kinetics and thermodynamics. *Energy* 211:118736. <https://doi.org/10.1016/j.energy.2020.118736>
30. Meng H, Wang S, Chen L, Wu Z, Zhao J (2015) Thermal behavior and the evolution of char structure during co-pyrolysis of platanus wood blends with different rank coals from northern China. *Fuel* 158:602–611. <https://doi.org/10.1016/j.fuel.2015.06.023>
31. Bhardwaj G, Kumar M, Mishra PK, Upadhyay SN (2021) Kinetic analysis of the slow pyrolysis of paper wastes. *Biomass Convers Bior.* <https://doi.org/10.1007/s13399-021-01363-7>
32. Chen J, Wang Y, Lang X, Ren X, Fan S (2017) Comparative evaluation of thermal oxidative decomposition for oil-plant residues via thermogravimetric analysis: thermal conversion characteristics, kinetics, and thermodynamics. *Bioresour Technol* 243:37–46. <https://doi.org/10.1016/j.biortech.2017.06.033>
33. Song Y, Hu J, Liu J, Evrendilek F, Buyukada M (2020) Catalytic effects of CaO, Al<sub>2</sub>O<sub>3</sub>, Fe<sub>2</sub>O<sub>3</sub>, and red mud on *Pteris vittata* combustion: emission, kinetic and ash conversion patterns. *J Clean Prod* 252:119646. <https://doi.org/10.1016/j.jclepro.2019.119646>
34. Xia B, Liu X, Song D, He X, Yang T, Wang L (2021) Evaluation of liquid CO<sub>2</sub> phase change fracturing effect on coal using fractal theory. *Fuel* 287:119569. <https://doi.org/10.1016/j.fuel.2020.119569>
35. Li J, Du Q, Sun C (2009) An improved box-counting method for image fractal dimension estimation. *Pattern Recogn* 42(11):2460–2469. <https://doi.org/10.1016/j.patcog.2009.03.001>
36. Boundzanga HM, Cagnon B, Roulet M, de Persis S, Vautrin ul C, Bonnamy S (2020) Contributions of hemicellulose, cellulose, and lignin to the mass and the porous characteristics of activated carbons produced from biomass residues by phosphoric acid activation. *Biomass Convers Bior.* <https://doi.org/10.1007/s13399-020-00816-9>
37. Shen DK, Gu S, Bridgwater AV (2010) Study on the pyrolytic behaviour of xylan-based hemicellulose using TG-FTIR and Py-GC-FTIR. *J Anal Appl Pyrolysis* 87(2):199–206. <https://doi.org/10.1016/j.jaap.2009.12.001>
38. Song Y, Li Q, Li F, Wang L, Hu C, Feng J, Li W (2019) Pathway of biomass-potassium migration in co-gasification of coal and biomass. *Fuel* 239:365–372. <https://doi.org/10.1016/j.fuel.2018.11.023>
39. Liu H, Xu L, Zhao D, Cao Q, Gao J, Wu S (2018) Effects of alkali and alkaline-earth metals and retention time on the generation of tar during coal pyrolysis in a horizontal fixed-bed reactor. *Fuel Process Technol* 179:399–406. <https://doi.org/10.1016/j.fuproc.2018.07.032>
40. Chen J, Zhang J, Liu J, He Y, Evrendilek F, Buyukada M, Xie W, Sun S (2020) Co-pyrolytic mechanisms, kinetics, emissions and products of biomass and sewage sludge in N<sub>2</sub>, CO<sub>2</sub> and mixed

- atmospheres. Chem Eng J 397:125372. <https://doi.org/10.1016/j.cej.2020.125372>
41. Huang H, Liu J, Liu H, Evrendilek F, Buyukada M (2020) Pyrolysis of water hyacinth biomass parts: bioenergy, gas emissions, and by-products using TG–FTIR and Py–GC/MS analyses. Energ Convers Manage 207:112552. <https://doi.org/10.1016/j.enconman.2020.112552>
  42. Protsenko VS, Danilov FI (2011) Activation energy of electrochemical reaction measured at a constant value of electrode potential. J Electroanal Chem 651(2):105–110. <https://doi.org/10.1016/j.jelechem.2010.12.014>
  43. Sarkheil H, Rahbari S (2019) Fractal geometry analysis of chemical structure of natural starch modification as a green biopolymeric product. Arab J Chem 12(8):2430–2438. <https://doi.org/10.1016/j.arabjc.2015.03.015>
  44. Wu Z, Yang W, Yang B (2018) Thermal characteristics and surface morphology of char during co-pyrolysis of low-rank coal blended with microalgal biomass: effects of *Nannochloropsis* and *Chlorella*. Bioresour Technol 249:501–509. <https://doi.org/10.1016/j.biortech.2017.09.196>
  45. Zhang J, Zou H, Liu J, Evrendilek F, Xie W, He Y, Buyukada M (2021) Comparative (co-)pyrolytic performances and by-products of textile dyeing sludge and cattle manure: deeper insights from Py–GC/MS, TG–FTIR, 2D–COS and PCA analyses. J Hazard Mater 401:123276. <https://doi.org/10.1016/j.jhazmat.2020.123276>

**Publisher's Note** Springer Nature remains neutral with regard to jurisdictional claims in published maps and institutional affiliations.